Article:

Electrical control of the Zeeman spin splitting in two-dimensional hole systems

E. Marcellina, A. Srinivasan, D. S. Miserev, O. P. Sushkov, Dimitrie Culcer, and A. R. Hamilton

School of Physics, The University of New South Wales, Sydney, Australia

A. F. Croxall, D. A. Ritchie, and I. Farrer

Cavendish Laboratory, University of Cambridge, J. J. Thomson Avenue, Cambridge CB3 0HE, United Kingdom

(Dated: June 29, 2018)

Semiconductor holes with strong spin-orbit coupling allow all-electrical spin control, with broad applications ranging from spintronics to quantum computation. Using a two-dimensional hole system in a GaAs quantum well, we demonstrate a new mechanism of electrically controlling the Zeeman splitting, which is achieved through altering the hole wave vector k. We find a threefold enhancement of the in-plane $g-$factor $g_\parallel(k)$. We introduce a new method for quantifying the Zeeman splitting from magnetoresistance measurements, since the conventional tilted field approach fails for two-dimensional systems with strong spin-orbit coupling. Finally, we show that the Rashba spin-orbit interaction suppresses the in-plane Zeeman interaction at low magnetic fields. The ability to control the Zeeman splitting with electric fields opens up new possibilities for future quantum spin-based devices, manipulating non-Abelian geometric phases, and realising Majorana systems in $p-$type superconductor systems.

The spin-orbit interaction couples a particle's spin to its motion, as described by the Hamiltonian $H_{\mathrm{SO}} = \frac{1}{2}\mu_B \boldsymbol{\sigma} . \boldsymbol{B}_{\mathrm{eff}}(\boldsymbol{k})$, where $\boldsymbol{\sigma}$, μ_B, $\boldsymbol{B}_{\mathrm{eff}}$, and $\boldsymbol{k}$ represent the Pauli matrices, the Bohr magneton, the effective spin-orbit magnetic field, and the motion wave vector, respectively [1]. The effective magnetic field $\boldsymbol{B}_{\mathrm{eff}}$ emerges from a relativistic transformation that occurs when a particle with spin $\boldsymbol{\sigma}$ is moving with wave vector $\boldsymbol{k}$ with respect to an electric field $\boldsymbol{F}$. The spin-orbit interaction has applications in spintronic devices and spin-based quantum computing, which rely on controlling spin via external electric fields $\boldsymbol{F}$ [2–13].

Here we report a new mechanism for electrically manipulating spin through the Zeeman interaction in two-dimensional (2D) holes. Unlike in electrons, the Zeeman splitting in holes is highly anisotropic, with the out-of-plane $g-$factor g_{zz} much larger than the in-plane one ($g_{zz} \gg g_\parallel$), and $g_\parallel$ strongly dependent on k. The ability to electrically control $g_\parallel$ is not only valuable for applications in spintronics and quantum computing, but also for engineering non-Abelian geometric phases [14, 15]. Moreover, in a hybrid semiconductor-superconductor system that can host Majorana fermions [16–22], a high tunability of the $g-$factor is desirable as it is then possible to use a magnetic field to drive the system from the trivial to the topological regime without quenching the superconductivity needed to support the Majorana mode.

Previous methods of tuning the $g-$factor in 2D systems relied on shifting the wave function from one material to another, either by pushing it across a heterointerface, or by using a graded composition quantum well [23]. Here we adopt a different approach, in which the $g-$factor is controlled not by shifting the wave function but by tuning the Fermi wave vector k_F of a 2D hole system. Owing to the spin$-3/2$ nature of the 2D holes [24], increasing k enhances the mixing between the occupied heavy hole and unoccupied light hole subbands, which then dramatically alters the in-plane $g-$factor $g_\parallel$. It is difficult to detect this variation of $g_\parallel$ with optical methods, since these detect bound excitons with a small and fixed k [25–27]. Instead we introduce a new approach based on magnetotransport in crossed magnetic fields, which shows that the spin splitting is linear in applied in-plane magnetic field, and can be varied by 300% as k_F is increased.

Our experiment was performed using an undoped 25 nm GaAs quantum well sandwiched between 300 nm $Al_{0.33}Ga_{0.67}As$ layers and grown along the (001) direction. Metal top and back gates supplied the 2D carriers and allowed the quantum well symmetry to be tuned arbitrarily [28]. The magnetotransport measurements were performed in a dilution refrigerator at a base temperature of $\sim$ 30 mK. The sample was mounted on an in-situ rotation system with an accuracy of $\pm 0.01^\circ$ [29]. Electrical measurements were carried out in the standard 4-terminal configuration with a source-drain current of 5 nA and a lock-in frequency of 17 Hz. The maximum 2D hole mobility was 1.5×10^6 cm^2 V^{-1} s^{-1} at density $p = 2.6 \times 10^{11}$ cm^{-2}.

To demonstrate the $k-$dependence of the Zeeman spin splitting, we tune the front- and backgate electric fields $(\overrightarrow{F}_{\mathrm{front}}, \overrightarrow{F}_{\mathrm{back}})$ on the quantum well to alter p (and hence k_F) while keeping the wave function in the quantum well center [Fig. 1(a)]. That is, we set the quantum well to be inversion-symmetric, so that the net electric field $\overrightarrow{F} \equiv F_z \hat{z} \equiv (\overrightarrow{F}_{\mathrm{front}} + \overrightarrow{F}_{\mathrm{back}})/2$ across the quantum well is zero, and there is no Rashba spin-orbit interaction [1, 30], see Section S1 of the Supplemental Material [31]. We then introduce an in-plane magnetic field $B_\parallel$ to cause an in-plane Zeeman spin splitting. To measure the change in spin splitting as a function of $B_\parallel$, we apply a small B_z to cause Shubnikov-de Haas oscillations, from which we measure the area of the Fermi surface. To this end, we tilt the sample at an angle θ with respect to the total magnetic field $\boldsymbol{B}$ [Fig. 1(b)]. The Shubnikov-de Haas oscillations at various θ for three different densities are shown in Figs. 1(c)-(e). At $\theta = 0^\circ$,
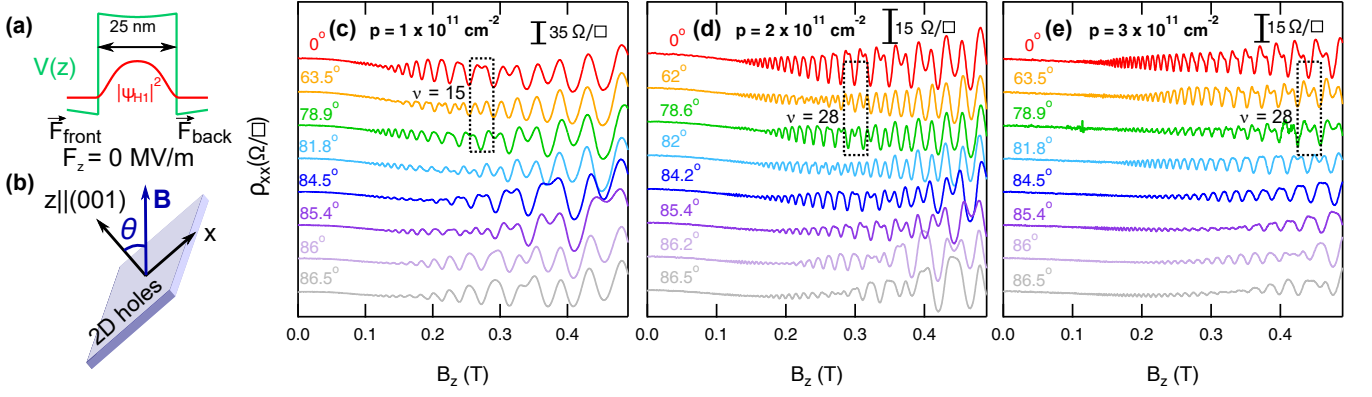
FIG. 1. (a) Schematic of the GaAs hole quantum well used in this work, where ψ_{H1} is the heavy hole wave function and $V(z)$ is the confinement potential controlled via electric fields $\overrightarrow{F}_{\text{front}}$ and $\overrightarrow{F}_{\text{back}}$ applied using the front and back gates, respectively. Here, the total electric field $\overrightarrow{F} = F_z \hat{z} \equiv (\overrightarrow{F}_{\text{front}} + \overrightarrow{F}_{\text{back}})/2 = 0$. (b) The device is tilted at an angle θ with respect to the applied magnetic field $\mathbf{B}$. (c)-(e) Magnetoresistance oscillations ρ_{xx} of the 2D holes in a symmetric quantum well at various tilt angles for three hole densities p. Due to the in-plane magnetic field, a resistance minimum gradually evolves into a maximum or vice versa, for example at $p = 1 \times 10^{11}$ cm^{-2} and $\nu = 15$ for angles $\theta = 0°$, 63.5°, 78.9° (see dashed box). (d)-(e) The effect of the in-plane magnetic field on the resistance becomes more pronounced as the 2D hole density increases: the transition between a resistance minimum and maximum occurs at smaller angles at higher densities (see dashed box). The traces have been offset for clarity.

for $0 \leq B_z \leq 0.25$ T, there is only one period of magnetoresistance oscillations ρ_{xx}, corresponding to a single spin-degenerate Fermi surface, where ρ_{xx} minima occurring only at even filling factors ν_{even}. At higher B_z, the out-of-plane Zeeman splitting $\propto g_{zz} B_z$ becomes visible, with ρ_{xx} minima also developing at odd filling factors ν_{odd}. Applying an in-plane magnetic field lifts the spin degeneracy even at low B_z, so that ρ_{xx} varies as a function of θ at a fixed B_z (and hence filling factor ν). The dashed box in Fig. 1(c) shows that the resistance maximum for $p = 1 \times 10^{11}$ cm^{-2} at $\nu = 15$ and $\theta = 0°$ evolves into a minimum as θ is gradually increased. Comparison between Figs. 1(d) and (e) shows that as p is increased, progressively smaller θ are required to cause this evolution. For $p = 2 \times 10^{11}$ cm^{-2}, the resistance minimum at $\nu = 28$ and $0°$ evolves into a weak minimum when θ is increased to 78.6° [see the dashed box in Fig. 1(d)]. By contrast, for $p = 3 \times 10^{11}$ cm^{-2} [see the dashed box in Fig. 1(e)], a weak minimum already develops at $\theta = 63.5°$ at $\nu = 28$. This comparison provides evidence that the in-plane Zeeman splitting is density-dependent. In fact, it was predicted that the in-plane Zeeman splitting in heavy holes, up to second order perturbation theory, is given by [1]:

$$
\begin{aligned}
E(k_{F\pm}) &= \frac{\hbar^2}{2m^*} k_{F\pm}^2 \pm Z\mu_B k_{F\pm}^2 B_\| \\
&\equiv \frac{\hbar^2}{2m^*} k_{F\pm}^2 \pm \frac{g_\|(k_{F\pm})}{2} \mu_B B_\|.
\end{aligned} \tag{1}
$$

where μ_B is the Bohr magneton and the Zeeman prefactor Z is detailed in Section S4.B of the Supplemental Material [39]. Thus, the effect of $B_\|$ is equivalent to changing the effective mass for the two spin subbands.

In 2D electrons, the $g-$factor can be extracted from tilted magnetic field measurements by finding the angle

θ_c at which the Zeeman energy $g\mu_B B$ equals half the cyclotron energy $(1/2)\hbar eB \cos \theta_c/m^*$ [41]. Assuming the electron effective mass m^* is known and g is isotropic ($g_{zz} = g_\|$), the $g-$factor is given by $g = (m_0 \cos \theta_c/m^*)$, where m_0 is the bare electron mass. However, this approach is not applicable for holes as the $g-$factor is highly anisotropic ($g_{zz} \gg g_\|$), and m^* depends on $B_\|$ (Eq. 1, see also Section S2 of the Supplemental Material [42]). Instead, here we examine the dependence of the magnetoresistance on $B_\|$ at a fixed B_z, and hence a fixed ν, to measure the area of the spin-split Fermi surfaces. To increase the visibility of the $B_\|-$induced magnetoresistance features against the smooth background, we define a dimensionless in-plane magnetoresistance $\Delta\bar{\rho}_{xx}$ at a given ν

$$
\Delta\bar{\rho}_{xx} = \Delta\bar{\rho}_{xx}(B_\|) \equiv \frac{\rho_{xx}^\nu - \rho_{xx}^{\nu+1}}{\rho_{xx}^\nu + \rho_{xx}^{\nu+1}}. \tag{2}
$$

The magnetoresistance $\bar{\rho}_{xx}$ [Fig. 2(a)-(c)] oscillates as a function of $B_\|$, with the frequency of the oscillations being independent of ν. Furthermore, the frequency increases with p.

The physical mechanism underlying the density-dependence of $\bar{\rho}_{xx}$ is illustrated in Figs. 2(d)-(f). We first consider the energy dispersion $E(k_x, k_y)$ in the absence of B_z. When $B_\| = 0$, the spin subbands HH1$_\pm$ are degenerate [Fig. 2(d)]. The effect of $B_\|$ on the energy dispersion is remarkably different for 2D holes than electrons. For 2D electrons, $B_\|$ splits all k states by $\Delta E_Z = g\mu_B B_\|$, whereas for 2D holes, $B_\|$ causes a $k-$dependent splitting of the HH1$_+$ and HH1$_-$ bands, so that $m_+ \neq m_-$ [Fig. 2(e)], where $m_\pm$ is the effective mass of the HH1$_\pm$ bands. The k-dependent spin splitting increases with $B_\|$, and the corresponding effective masses m_+ and m_- diverge
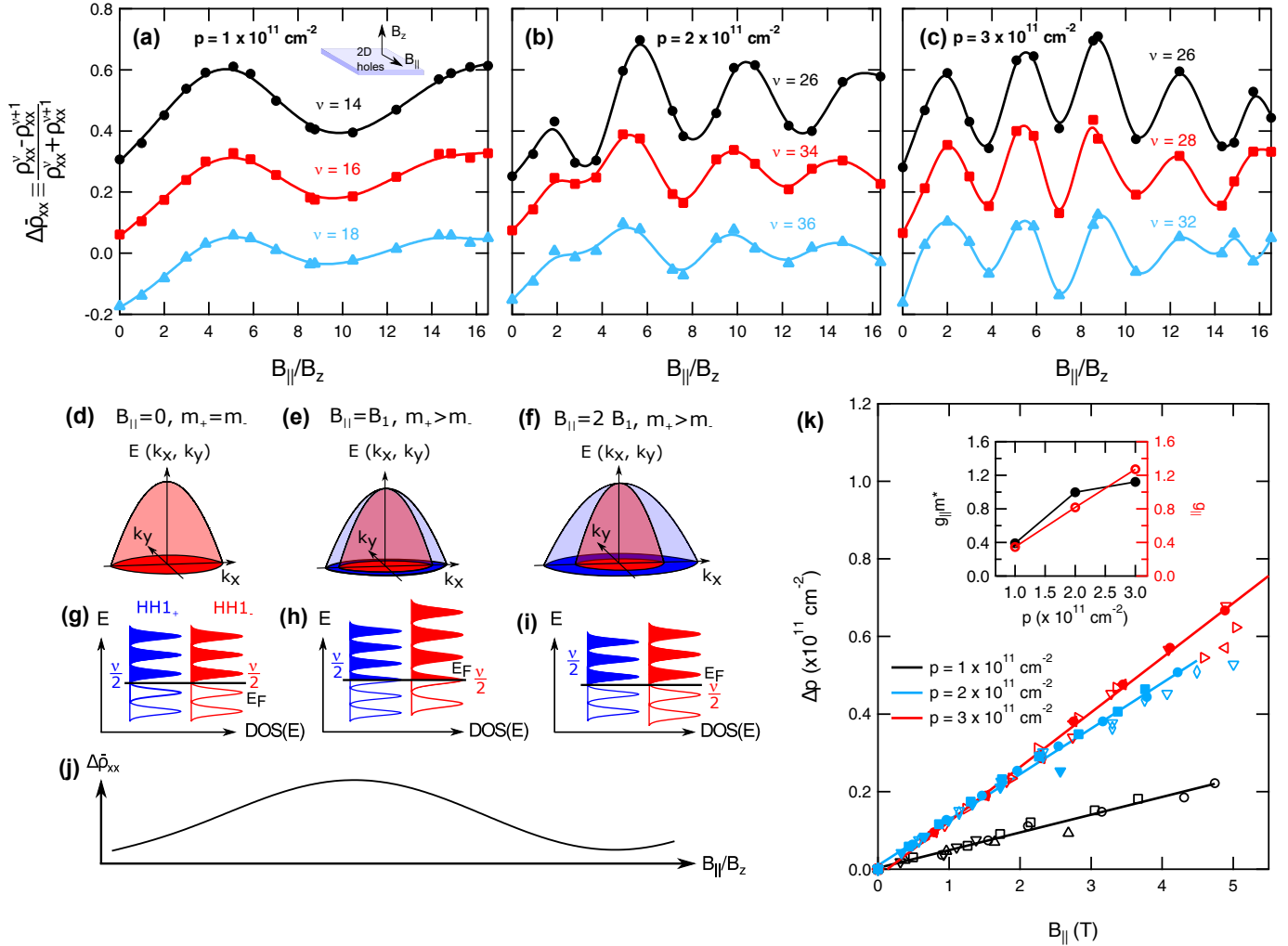
FIG. 2. (a)-(c) Resistance oscillations $\Delta\bar{\rho}_{xx} = \Delta\bar{\rho}_{xx}(B_\parallel) \equiv (\rho_{xx}^\nu - \rho_{xx}^{\nu+1})/(\rho_{xx}^\nu + \rho_{xx}^{\nu+1})$ at various filling factors ν for different p. (d)-(f) Schematic of the energy band dispersion $E(k_x, k_y)$, showing how the k-dependent Zeeman splitting, where $k \equiv \sqrt{k_x^2 + k_y^2}$, changes the effective masses m_+ and m_- in the two bands. (g)-(i) Schematic of the Landau levels corresponding to the band structure in (d)-(f) for an even ν. The shaded regions refer to the filled Landau levels. As $B_\parallel$ is increased from 0 T to $B_\parallel = B_1 > 0$ T, the Landau level spacing in the two spin-split bands changes due to the different masses. (j) The in-plane magnetoresistance $\Delta\bar{\rho}_{xx}$ arises from the change in the density of states at the Fermi energy as illustrated in (d)-(f). (k) The difference in the hole density of the two spin split bands Δp as a function of $B_\parallel$ for different p, as indicated by the three different colours. The inset shows $g_\parallel m^*$ (solid black line with solid circles) extracted using Eq. 1. Using the effective masses obtained from 6×6 $\boldsymbol{k}.\boldsymbol{p}$ calculations [43], we find $g_\parallel$ (solid red line with open circles), which increases linearly with density.

further [Fig. 2(f)] with $B_\parallel$. When B_z is finite, Landau levels form, where the energy separation between the Landau levels depends on the effective mass, and hence on $B_\parallel$. When $B_\parallel = 0$, the HH1$_\pm$ Landau levels are spin degenerate, $m_+ = m_-$, and the number of occupied Landau levels is identical in the HH1$_+$ and HH1$_-$ subbands ($\nu_+ = \nu_-$) [Fig. 2(g)]. When $B_\parallel \neq 0$, m_+ diverges from m_-, changing the spacing of Landau levels in the HH1$_+$ and HH1$_-$ bands. Thus, the density of states at the Fermi energy E_F as ν_+ and ν_- changes with $B_\parallel$ [Figs. 2(h)-(i)]. Assuming that the change $\Delta\nu_\pm$ in the occupancy of the HH1$_\pm$ Landau levels is much smaller than ν ($\Delta\nu_\pm/\nu \ll 1$), the Landau level occupation changes in

pairs, i.e. $\Delta\nu_+ = -\Delta\nu_-$ [Fig. 2(g)].

The change in the density of states at E_F causes $\Delta\bar{\rho}_{xx}$ to oscillate as a function of $B_\parallel$ at a fixed B_z. When E_F coincides (does not coincide) with a Landau level, a maximum (minimum) in $\Delta\bar{\rho}_{xx}$ develops [Fig. 2(j)]. Since one oscillation period of $\Delta\bar{\rho}_{xx}$ corresponds to $|\Delta\nu_\pm| = 1$, the spin splitting after moving n $\bar{\rho}_{xx}(B_\parallel)$ resistance peaks away from the symmetry point is given by:

$$\frac{\nu/2 + n\Delta\nu_\pm}{\nu} = \frac{p_\pm}{p}, \quad (3)$$

where $p_\pm$ is the spin-split densities. Note that although Eq. 3 is exact for parabolic and isotropic bands (see Sec-

tion S2 of the Supplemental Material [42]), it also holds for non-parabolic and/or anisotropic bands as long as $\Delta\nu_\pm/\nu \ll 1$ (see Sections S3 and S4 of the Supplemental Material [44]). We remark that the resistance oscillations $\Delta\bar\rho_{xx}(B_\parallel)$ are analogous to Shubnikov-de Haas oscillations: in conventional Shubnikov-de Haas oscillations, the Landau level spacing eB_z/m^* is controlled by varying B_z, whereas the oscillations $\Delta\bar\rho_{xx}(B_\parallel)$ are caused by varying $m_\pm$.

We use Eq. 3 to extract from $\Delta\bar\rho_{xx}(B_\parallel)$ the change in the area of the spin-split Fermi surfaces, and hence the spin splitting Δp, as a function of $B_\parallel$. We obtain Δp for multiple values of ν, as indicated by the symbols in Fig. 2(k). The spin splitting is independent of ν, and increases linearly with $B_\parallel$. To obtain $g_\parallel = g_\parallel(k_F)$ from Δp, we use the dispersion relation in Eq. 1 and obtain $Z\mu_B = 1.37,\ 1.88,\ 1.95 \times 10^{-18}$ meV m^2 T^{-1} and $g_\parallel(k_F)m^*/m_0 = 0.39,\ 0.99$, and 1.18, for $p = 1,\ 2$, and 3×10^{11} cm^{-2}, respectively (shown by the solid black line and solid circles in the inset to Fig. 2(k)). Using the effective masses obtained from 6×6 **k.p** calculations [43], i.e. $m^* = 1.13, 1.22$, and $0.88\ m_0$ for $p = 1,\ 2$, and 3×10^{11} cm^{-2} respectively, we find $g_\parallel = 0.34,\ 0.82$, and 1.26 (shown by the solid red line and open circles in the inset to Fig. 2(k)). These values of $g_\parallel$ are of the same order of magnitude as the predicted values for 2D hole systems [46, 47]. It is also interesting to note that the values of $g_\parallel$ we measure here are consistent with the experimental results for quasi-one dimensional hole systems [48–50].

Finally, we investigate the interplay of Rashba and Zeeman interactions by repeating the tilted magnetic field measurements with a finite electric field F_z applied across the quantum well and a fixed density of $p = 2 \times 10^{11}$ cm^{-2}. Figs. 3(a) and (b) show Shubnikov-de Haas oscillations for $F_z = 0$ MV/m and $F_z = 0.43$ MV/m. When the quantum well is symmetric ($F_z = 0$ MV/m), the Rashba splitting is zero, and the magnetoresistance at $\theta = 0°$ shows a single oscillation period at low B_z, with each Landau level being doubly degenerate. In this case, $B_\parallel$ has a strong influence on the Shubnikov-de Haas oscillations, as shown by the dashed box. By contrast, when F_z is large ($F_z = 0.43$ MV/m), the magnetoresistance at $\theta = 0$ shows a beating due to the Rashba splitting even at $B_\parallel = 0$. A Fourier transform of the $\theta = 0°$ oscillations shows a large Rashba splitting of $\Delta p/p = 40\%$ (see Section S1 of the Supplemental Material [31]). This Rashba interaction dramatically suppresses the effects of $B_\parallel$ on the Shubnikov-de Haas oscillations: the positions of maxima and minima for $\theta = 0°$ and $\theta = 62°$ are practically identical and only at high tilt angles, $\theta > 80°$, do the oscillation minima evolve into maxima or vice versa.

It is challenging to perform a complete quantitative analysis to extract Δp and $g_\parallel$ when both Rashba and Zeeman interactions are finite. The method of counting the periodic Landau level population/depopulation becomes invalid when $\Delta\nu/\nu \ll 1$ is violated, which is the case with $F_z = 0.43$ MV/m. There is currently no analyt-
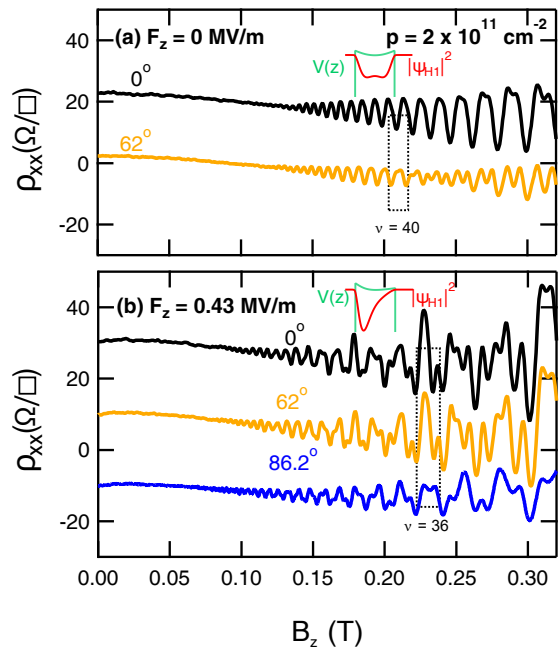

FIG. 3. (a) In the absence of Rashba splitting ($F_z = 0$ MV/m), the magnetoresistance minima change into maxima (or vice versa) when θ is increased from $0°$ to $62°$, as highlighted in the dashed box for $\nu = 40$. (b) At $F_z = 0.43$ MV/m, the Shubnikov-de Haas oscillations are far less affected by θ: when θ is increased from $0°$ to $62°$ the positions of the minima and maxima remain almost unchanged, and only when θ is large ($\theta > 80°$), do the resistance minima evolve into maxima (the dashed box highlights $\nu = 36$). Here, $p = 2 \times 10^{11}$ cm^{-2}. The shape of the potential profile and ground state envelope wavefunction are shown in green and red. The traces are offset for clarity.

ical or numerical modeling of 2D holes under the Rashba spin-orbit interaction in tilted magnetic field configuration against which we can compare our data. Such calculations are extremely challenging due to the combination of quantum confinement, the four-component hole spinor [51], heavy hole-light hole coupling, as well as the simultaneous inclusion of B_z and $B_\parallel$ [52]. To get a qualitative understanding of Fig. 3, we present a minimal model for the spin splitting when both Rashba and in-plane Zeeman interactions are present at $B_z = 0$ T (see Section S5 of the Supplemental Material [42]). The suppression of $g_\parallel$ in Fig. 3 is due to the Rashba interaction dominating over the in-plane Zeeman interaction. In this limit, the effect of $B_\parallel$ is to offset the center of the Fermi surfaces from $k = 0$, without changing the areas appreciably. This is because the Rashba and in-plane Zeeman interactions have similar functional forms, i.e. $(k_-^3\sigma_+ + k_+^3\sigma_-)$ and $(k_-^2 B_-\sigma_+ + k_+^2 B_+\sigma_-)$, respectively. We note that in the opposite limit, where the in-plane Zeeman interaction is much larger than the Rashba interaction, $g_\parallel$ reverts to its value at zero Rashba interaction (Fig. S3(a) of the Supplemental Material [42]).

In summary, we have demonstrated all-electrical con-

trol of the in-plane Zeeman splitting of 2D holes by separately varying the 2D hole density p and the electric field F_z across the quantum well. We have developed a novel method to quantify the Zeeman splitting from the tilted magnetic field measurements. This new method can in principle be generalized to other 2D materials with an anisotropic $g-$factor ($g_\parallel \neq g_{zz}$) as long as the confinement potential is inversion-symmetric. By tracking the evolution of the Landau levels as a function of $B_\parallel$, we show that the in-plane Zeeman splitting of 2D holes is proportional to p, and that $g_\parallel$ can be tripled. However, the experimental and calculated values of $g_\parallel$ diverge by up to a factor of 3, which is likely due to exchange and correlations. We have also shown that a strong F_z can suppress $g_\parallel$, although a complete quantitative analysis for extracting $g_\parallel$ in the case of finite F_z is beyond the scope of the present work. The ability to electrically tune $g_\parallel$ will be useful for designing spin-based devices, such as spin-transistors, spin-orbit qubits, quantum logic gates, and hybrid superconductor-semiconductor systems hosting Majorana modes.

ACKNOWLEDGEMENTS

[1] R. Winkler, *Spin Orbit Coupling Effects in Two-Dimensional Electron and Hole Systems* (Springer-Verlag, Berlin, 2003).
[2] S. Datta and B. Das, Appl. Phys. Lett. **56**, 665 (1990).
[3] I. Žutić, J. Fabian, and S. D. Sarma, Rev. Mod. Phys. **76**, 323 (2004).
[4] D. Loss and D. P. DiVincenzo, Phys. Rev. A **57**, 120 (1998).
[5] S. A. Wolf, D. D. Awschalom, R. A. Buhrman, J. M. Daughton, S. von Molnár, M. L. Roukes, A. Y. Chtchelkanova, and D. M. Treger, Science **294**, 1488 (2001).
[6] D. D. Awschalom, L. C. Bassett, S. D. Dzurak, E. L. Hu, and J. R. Petta, Science **339**, 1174 (2013).
[7] K. C. Nowack, F. H. L. Koppens, Y. V. Nazarov, and L. M. K. Vandersypen, Science **318**, 1430 (2007).
[8] D. V. Bulaev and D. Loss, Phys. Rev. Lett. **98**, 097202 (2007).
[9] S. Nadj-Perge, S. M. Frolov, E. P. A. M. Bakkers, and L. P. Kouwenhoven, Nature **468**, 1084 (2010).
[10] V. S. Pribiag, S. Nadj-Perge, S. M. Frolov, J. W. G. van den Berg, I. van Weperen, S. R. Plissard, E. P. A. M. Bakkers, and L. P. Kouwenhoven, Nat. Nanotechnol. **8**, 170 (2013).
[11] R. Maurand, X. Jehl, D. K. Patil, A. Corna, H. Bohuslavskyi, R. Laviéville, L. Hutin, S. Barraud, M. Vinet, M. Sanquer, and S. De Franceschi, Nat. Commun. **7**, 1 (2016).
[12] J. Salfi, J. A. Mol, D. Culcer, and S. Rogge, Phys. Rev. Lett. **116**, 246801 (2016).
[13] J.-T. Hung, E. Marcellina, B. Wang, A. R. Hamilton, and D. Culcer, Phys. Rev. B **95**, 195316 (2017).
[14] J. C. Budich, D. G. Rothe, E. M. Hankiewicz, and B. Trauzettel, Phys. Rev. B. **85**, 205425 (2012).
[15] T. Li, L. A. Yeoh, A. Srinivasan, O. Klochan, D. A. Ritchie, M. Y. Simmons, O. P. Sushkov, and A. R. Hamilton, Phys. Rev. B **93**, 205424 (2016).
[16] J. Alicea, Y. Oreg, G. Refael, F. von Oppen, and M. P. A. Fisher, Nat. Phys. **7**, 412 (2010).
[17] R. M. Lutchyn, T. D. Stanescu, and S. Das Sarma, Phys. Rev. Lett. **106**, 127001 (2011).
[18] L. Mao, M. Gong, E. Dumitrescu, S. Tewari, and C. Zhang, Phys. Rev. Lett. **108**, 177001 (2012).
[19] V. Mourik, K. Zuo, S. M. Frolov, S. R. Plissard, E. P. A. M. Bakkers, and L. P. Kouwenhoven, Science **336**, 1003 (2012).
[20] L. P. Rokhinson, X. Liu, and J. K. Furdyna, Nat. Phys. **8**, 795 (2012).
[21] S. Vaitiek.nas, M. T. Deng, J. Nygård, P. Krogstrup, and C. M. Marcus, "Effective $g-$factor in Majorana Wires," (2017), arXiv:1710.04300.
[22] J. Liang and Y. Lyanda-Geller, Phys. Rev. B **95**, 201404 (2017).
[23] G. Salis, Y. Kato, K. Ensslin, D. C. Driscoll, A. C. Gossard, and D. D. Awschalom, Nature **414**, 619 (2001).
[24] J. M. Luttinger, Phys. Rev. **102**, 1030 (1956).
[25] M. Syperek, D. R. Yakovlev, A. Greilich, J. Misiewicz, M. Bayer, D. Reuter, and A. D. Wieck, Phys. Rev. Lett. **99**, 187401 (2007).
[26] M. Kugler, T. Andlauer, T. Korn, A. Wagner, S. Fehringer, R. Schulz, M. Kubová, C. Gerl, D. Schuh, W. Wegscheider, P. Vogl, and C. Schüller, Phys. Rev. B **80**, 035325 (2009).
[27] C. Gradl, M. Kempf, D. Schuh, D. Bougeard, R. Winkler, C. Schüller, and T. Korn, Phys. Rev. B **90**, 165439 (2014).
[28] A. F. Croxall, B. Zheng, F. Sfigakis, K. Das Gupta, I. Farrer, C. A. Nicoll, H. E. Beere, and D. A. Ritchie, Appl. Phys. Lett. **102**, 082105 (2013).
[29] L. A. Yeoh, A. Srinivasan, T. P. Martin, O. Klochan, A. P. Micolich, and A. R. Hamilton, Rev. Sci. Instrum. **81**, 113905 (2010).
[30] Y. A. Bychkov and E. I. Rashba, J Phys. C: Solid State **17**, 6039 (1984).
[31] See Supplemental Material at [URL] for details on tuning the quantum well asymmetry, which includes Refs. [32–38].
[32] G. Dresselhaus, Phys. Rev. **100**, 580 (1955).
[33] P. T. Coleridge, R. Stoner, and R. Fletcher, Phys. Rev. B **39**, 1120 (1989).
[34] R. Winkler, S. J. Papadakis, E. P. De Poortere, and M. Shayegan, Phys. Rev. Lett. **84**, 713 (2000).

[35] S. Keppeler and R. Winkler, Phys. Rev. Lett. **88**, 046401 (2002).

[36] B. Habib, M. Shayegan, and R. Winkler, Semicond. Sci. Tech. **23**, 064002 (2009).

[37] T. Li, B. Horovitz, and O. P. Sushkov, Phys. Rev. B **93**, 235316 (2016).

[38] E. Marcellina, A. R. Hamilton, R. Winkler, and D. Culcer, Phys. Rev. B **95**, 075305 (2017).

[39] See Supplemental Material at [URL] for additional details and calculations, which includes Ref. [40].

[40] A. Baldereschi and N. Lipari, Phys. Rev. B **8**, 2697 (1973).

[41] F. F. Fang and P. J. Stiles, Phys. Rev. **174**, 823 (1968).

[42] See Supplemental Material at [URL] for detailed calculations.

[43] S. Birner, T. Zibold, T. Andlauer, T. Kubis, M. Sabathil, A. Trellakis, and P. Vogl, IEEE Trans. Electron Dev. **54**, 2137 (2007).

[44] See Supplemental Material at [URL] for a detailed derivation of Eq. 3, which includes Ref. [45].

[45] O. Gunawan, Y. P. Shkolnikov, E. P. De Poortere, E. Tutuc, and M. Shayegan, Phys. Rev. Lett. **93**, 246603 (2004).

[46] T. Kernreiter, M. Governale, and U. Zülicke, Phys. Rev. Lett. **110**, 026803 (2013).

[47] D. S. Miserev and O. P. Sushkov, Phys. Rev. B **95**, 085431 (2017).

[48] D. S. Miserev, A. Srinivasan, O. A. Tkachenko, V. A. Tkachenko, I. Farrer, D. A. Ritchie, A. R. Hamilton, and O. P. Sushkov, Phys. Rev. Lett. **119**, 116803 (2017).

[49] F. Nichele, A. N. Pal, R. Winkler, C. Gerl, W. Wegscheider, T. Ihn, and K. Ensslin, Phys. Rev. B **89**, 081306(R) (2014).

[50] A. Srinivasan, D. S. Miserev, K. L. Hudson, O. Klochan, K. Muraki, Y. Hirayama, D. Reuter, A. D. Wieck, O. P. Sushkov, and A. R. Hamilton, Phys. Rev. Lett. **118**, 146801 (2017).

[51] R. Winkler, Phys. Rev. B **71**, 113307 (2005).

[52] L. A. Yeoh, A. Srinivasan, O. Klochan, R. Winkler, U. Zülicke, M. Y. Simmons, D. A. Ritchie, M. Pepper, and A. R. Hamilton, Phys. Rev. Lett. **113**, 236401 (2014).